Quantifying the impact of synoptic circulation patterns on ozone variability in North China from April-October 2013-2017

Jingda Liu[1,2], Lili Wang[2,4], Mingge Li[2,5], Zhiheng Liao[6], Yang Sun[2], Tao Song[2], Wenkang Gao[2], Yonghong Wang[4], Yan Li[7], Dongsheng Ji[2], Bo Hu[2], Veli-Matti Kerminen[4], Yuesi Wang[1,2,3,5], Markku Kulmala[4]

[1]Department of Atmospheric Physics, Nanjing University of Information Science & Technology, Nanjing 210044, China

[2]State Key Laboratory of Atmospheric Boundary Layer Physics and Atmospheric Chemistry (LAPC), Institute of Atmospheric Physics, Chinese Academy of Sciences, Beijing 100029, China

[3]Centre for Excellence in Atmospheric Urban Environment, Institute of Urban Environment, Chinese Academy of Science, Xiamen, Fujian 361021, China

[4]Institute for Atmospheric and Earth System Research / Physics, Faculty of Science, University of Helsinki, Finland

[5]University of Chinese Academy of Sciences, Beijing 100049, China

[6]School of Atmospheric Sciences, Sun Yat-sen University, Guangzhou, Guangdong, China

[7]Fangshan Meteorological Bureau, Beijing, 102488, China

Correspondence to: Lili Wang (wll@mail.iap.ac.cn)

Abstract

The ozone variation characteristics and the impact of synoptic and local meteorological factors in North China were analysed quantitatively during the warm season from 2013 to 2017 based on multi-city in situ ozone and meteorological data as well as meteorological reanalysis. The domain-averaged maximum daily 8-h running average O_3 (MDA8 O_3) concentration was 122±11 μg m^{-3}, with an increase rate of 7.88 μg m^{-3} $year^{-1}$, and the three most highly polluted months were closely related to synoptic circulation patterns variations , which were June (149 μg m^{-3}), May (138 μg m^{-3}) and July (132 μg m^{-3}). Twenty-six weather types (merged into 5 weather categories) were objectively identified using the Lamb-Jenkinson method. The highly-polluted weather categories included S-W-N directions (geostrophic wind direction diverts from south to north), LP (low-pressure related weather types) and C (cyclone type, controlled by low pressure center), and the corresponding domain-averaged MDA8 O_3 concentrations were 122, 126 and 128 μg m^{-3}, respectively. Based on the frequency and intensity changes of synoptic circulation patterns, 39.2% of the inter-annual domain-averaged O_3 increase from 2013 to 2017 was attributed to synoptic changes, and intensity of synoptic circulation patterns was the dominant factor. Using synoptic classification and local meteorological factors, the segmented synoptic-regression approach was established to evaluate and forecast daily ozone variability on an urban scale. The results showed that this method is practicable in most cities and that the dominant factors are the maximum temperature, southerly winds, relative humidity on the previous day and on the same day, and total cloud cover. Overall, 41-63% of the day-to-day variability of MDA8 O_3 concentrations was due to local meteorological variations in most cities over North China, except for two cities: QHD (Qinhuangdao) at 34% and ZZ (Zhengzhou) at 20%. Our quantitative exploration of the synoptic and local meteorological

factors influencing both inter-annual and day-to-day ozone variability will provide a scientific basis for evaluating emission reduction measures since the national and local governments have implemented a series of measures to mitigate air pollution in North China.

1 Introduction

Tropospheric ozone (O_3) is one of the air pollutants of greatest concern due to its considerable harm to human health and vegetation (Kinney, 2008; Fleming et al., 2018; Mills et al., 2018). O_3 is formed through nonlinear interactions between NO_x and volatile organic compounds in combination with sunlight (Monks et al., 2009; Monks et al., 2015). Thus, ozone levels are controlled by precursors and meteorological conditions. With industrialization advancement and rapid economic growth, North China is one of the most populated and most polluted regions in the world. The national and local governments have implemented a series of measures to reduce emissions since 2013, and although $PM_{2.5}$ has decreased significantly, O_3 pollution is still serious in this region (Lu et al., 2018; Li et al., 2019). Several studies have explored the variation in summer ozone in China (He et al., 2017; Liao et al., 2017; Lu et al., 2018; Li et al., 2019), but systematic research aiming at quantifying the evolution characteristics of ozone and meteorological impacts and contributions are still lacking for the entire warm season (April-October) in the five years (2013-2017) during which the Action Plan for Air Pollution Prevention and Control (www.gov.cn/zwgk/2013-09/12/content_2486773.htm) was implemented. This lack of analysis prevents a clear understanding of the effect of emission reduction measures on ozone in North China.

Meteorological factors affect ozone levels through a series of complex combinations of processes, including emission, transport, chemical transformations and removal (Chan and Yao, 2008; Jacob and Winner, 2009; Lu et al., 2019). Meteorological conditions are the primary factor determining day-to-day variations in pollutant concentrations over China (He et al., 2016; He et al., 2017), whereas long-term O_3 trends are influenced both by climatological (weather types, temperature, humidity, and radiation, etc.) and environmental factors (changes in anthropogenic and natural sources). Therefore, the impact of reduced anthropogenic emissions on O_3 variation can be estimated more accurately if we are able to quantify the meteorological influence.

Synoptic meteorological conditions have an important effect on regional ozone distribution and variation (Shen et al., 2015). A given synoptic circulation pattern represents a particular range of meteorological conditions; therefore, synoptic classification is a useful method for gaining insight into the impact of meteorology on ozone levels on the regional scale. Previous studies have proved a significant connection between the weather type and surface O_3 concentration, but the relation between these two quantities varies in different regions differences in the topography, pollution source, local circulation, etc (Moody et al., 1998; Cooper et al., 2001; Hegarty et al., 2007; Demuzere et al., 2009; Monks et al., 2009; Wang et al., 2009a; Zhang et al., 2012; Zhang et al., 2013; Pope et al., 2016; Liao et al., 2017). For example, based on the Lamb-Jenkinson weather typing technique, Demuzere et al. (2009) demonstrated higher surface O_3 concentrations in summer in an easterly weather type at a rural site in Cabauw, Netherlands, whereas the opposite result was obtained by Liao et al. (2017) in the Yangtze River Delta region in eastern China. Therefore, synoptic classification and its relationship with O_3 need to be explored separately in different regions. In addition, based on synoptic classification, Comrie and Yarnal (1992) and Hegarty et al. (2007) suggested a reconstructed pollutant concentration (caused by synoptic influence) algorithm, which can separate climatological and environmental variability in environmental data. It was found that 46% and 50% of the inter-annual variability in the O_3 concentration was reproduced in the northeastern United States (Hegarty et al., 2007) and Hong Kong (Zhang et al., 2013), respectively, by taking into account the inter-annual changes in the frequency and intensity of synoptic patterns.

At an urban scale, the daily variation in ozone is affected by both synoptic and local meteorological factors. Quantifying the contribution of local meteorological factors to the day-to-day variation in ozone will a provide scientific basis and guidance for reasonable ozone reduction measures, and clarifying and quantifying the relationship between meteorological factors and ozone is vital for daily ozone pollution potential forecasts. A weather type classification prior to the regression analysis is superior to a simple linear regression approach (Eder et al., 1994; Barrero et al., 2006; Demuzere et al., 2009; Demuzere and van Lipzig, 2010), and the synoptic-regression-based algorithm can reproduce the observed O_3 distributions and provide a better parameterization to promote understanding of the dependence of ozone on meteorological factors in a given urban region.

Overall, in this study, we explore how the maximum daily 8-h running average O_3 (MDA8 O_3) concentration varies and quantify the contributions of synoptic and local meteorological conditions to ozone variability in North China (58 cities covering Hebei, Shanxi, Shandong, and Henan Provinces and Beijing and Tianjin municipalities) from April-October 2013-2017. Our specific goals are 1) to demonstrate characteristics and variation trends in surface MDA8 O_3 concentration; 2) to classify the predominant weather types and meteorological mechanism underlying regional ozone levels and variability; 3) to quantify the contribution of changes in synoptic circulation patterns (frequency and intensity) to the inter-annual variability of the O_3 concentration; and 4) to quantify the contributions of local meteorological factors to the day-to-day variation in O_3 levels, then identify the prominent meteorological variables and construct the O_3 potential forecast model for major cities..

2 Data and methods

2.1 Ozone and $PM_{2.5}$ data

The hourly O_3 and $PM_{2.5}$ data during April-October, 2013-2017 were derived from the National Urban Air Quality Real-time Publishing Platform (http://106.37.208.233:20035/). According to technical regulation for ambient air quality assessment (HJ 663-2013, http://www.mee.gov.cn/), the MDA8 O_3 concentration was calculated for each monitoring site based on the hourly data from 08:00-24:00 for the days with no <14-h measurements. If less than 14 hours of valid data are available, the results are still valid if the MDA8 O_3 concentration exceeds the national concentration limit standard. Each city has at least two monitoring sites, and the city MDA8 O_3 levels are the corresponding averages over all sites in that city. MDA8 O_3 values were collected in only 14 cities for the time period 2013-2017 and in an additional 44 cities for the time period 2015-2017, with detailed information shown in Fig. 1 and Table S1. The original unit of the ozone observations is μg m^{-3}, and the converted coefficient from mixing ratios (unit: ppbv) to μg m^{-3} is a constant (e.g., 0.5 at temperature of 25 °C and pressure of 1013.25 hPa). In this study, we will use the original unit. Unless otherwise noted, the analysis of O_3 refers to MDA8 O_3 during April-October in this paper.

2.2 Meteorological data

Gridded-mean sea level pressure data, 10-meter U and V wind components (U_{10} and V_{10}, respectively), boundary layer height (BLH) and 2-meter temperature (T_2) with a 1° horizontal resolution and vertical velocity (ω) from 1000-100 hPa (27 levels) and wind divergence (div) from 1000-850 hPa (7 levels) in 6-h intervals (Beijing time 02, 08, 14 and 20) for 2013-2017 were obtained from the European Centre for Medium Weather Forecast Re-analysis Interim (ERA-Interim).

Four measurements per day for temperature (T), relative humidity (RH), total cloud cover (TCC), rain, wind speed (ws) and direction (wd), and pressure (pre) in 58 cities during April-October in 2013-2017 were obtained from China Meteorological Administration in the Meteorological Information Combine Analysis and Process System (MICAPS). Then, daily-mean meteorological factors were averaged from four measurements (scalar averaging for most factors and vector averaging for wind speed and wind direction, which involved using the u component (U) and v component (V) for averaging). The meteorological station with a minimum distance from the city center was chosen.

2.3 Lamb-Jenkinson circulation typing

The Lamb-Jenkinson weather type approach (Lamb, 1972; Yarnal, 1993; Conway and Jones, 1998; Trigo and Dacamara, 2000; Mckendry et al., 2006; Demuzere et al., 2009; Russo et al., 2014; Santurtún et al., 2015; Pope et al., 2016; Liao et al., 2017) has been widely employed to classify the synoptic circulation. On the basis of the Lamb-Jenkinson method, the weather type circulation pattern for a given day is described using the locations of the high- and low-pressure centers that identify the direction of the geostrophic flow; the method uses coarsely gridded pressure data on a 16-point moveable grid (Demuzere et al., 2009). In our study, the North China is set as the center. The specific schematic diagram is shown in Fig. 1a. The daily mean sea level pressure data are averaged among four time points to determine the daily weather type. The detailed classification procedure can be found in Trigo and Dacamara (2000) and in the supplementary information (Text S1).

2.4 Reconstruction of O_3 concentration based on weather types

To quantify the interannual variability captured by the surface circulation pattern variations, Comrie and Yarnal (1992) suggested an algorithm to separate synoptic and non-synoptic variability in environmental data; by multiplying the overall mean value of a particular pattern by the occurrence frequency of that type of year, the climate signal can be obtained as follows:

$$\overline{\overline{O}}_{3\,m}(\mathrm{fre}) = \sum_{k=1}^{26} \overline{O_{3k}} F_{km} \qquad (1)$$

Here $\overline{\overline{O}}_{3\,m}(\mathrm{fre})$ is the reconstructed mean MDA8 O_3 concentration influenced by frequency changes of weather types during April-October for the year m, $\overline{O_{3k}}$ is the 5-year mean MDA8 O3 concentration per weather type k, and F_{km} is the occurrence frequency of weather type k during April-October for the year m.

Hegarty et al. (2007) suggested that variations in the circulation patterns are attributed not only to frequency changes but also to intensity variations, and that considering these two changes can better separate environmental and climate-related contributions in the inter-annual ozone variation. As a result, Equation (1) is modified into the following form:

$$\overline{\overline{O}}_{3\,m}(\mathrm{fre} + \mathrm{int}) = \sum_{k=1}^{26} (\overline{O_{3k}} + \Delta O_{3km}) F_{km} \qquad (2)$$

where $\overline{\overline{O}}_{3\,m}(\mathrm{fre} + \mathrm{int})$ is the reconstructed mean MDA8 O_3 concentration influenced by the frequency and intensity changes of circulation patterns during April-October for the year m; ΔO_{3km} is the modified difference on the fitting line, obtained through a linear fitting of the annual MDA8 O_3

concentration anomalies (ΔO_3) to the circulation intensity index (CII) for circulation pattern k in the year m. ΔO_{3km} represents the part of annual observed ozone oscillation caused by the intensity in each circulation pattern. Hegarty et al. (2007) used the domain-averaged sea level pressure (mslp) to represent the CII.

To better characterize intensity variations, we added 5 circulation intensity indexes: the difference between the highest pressure and lowest pressure (gradient), the center pressure of the highest pressure system (max slp), the center pressure of the lowest pressure system (min slp), the distance from the highest pressure centers to the study city (dis max), and the distance from the lowest pressure centers to the study city (dis min). The effective circulation intensity index (ECII) is one of the 6 CIIs and has the strongest correlation coefficient (r) between CII and ΔO_3. Thus, ECII is used in Equation (2) to calculate ΔO_{3km}. All CIIs for 14 cities were calculated based on 10°×10° grids covering North China (32°N-42°N, 110°E-120°E). One example of ΔO_{3km} (weather type C in ZJK) is shown in Fig. 7a. Min slp has the highest r (-0.97) among the 6 CIIs in type C in ZJK; therefore, min slp is the ECII.

2.5 The segmented synoptic-regression approach and model validation

The utilization of a segmented synoptic-regression approach can aid in minimizing the errors when using a linear regression to model a nonlinear relationship and effectively forecast ozone variation (Robeson and Steyn, 1990; Liu et al., 2007; Demuzere and van Lipzig, 2010; Liu et al., 2012). Based on local monitored meteorological data, their 24-h time lag values and weather type classifications, stepwise linear regression was used in every weather category to construct the ozone potential forecast model. The details of the main methods are shown in Text S2. Notably, in this research, after excluding the missing data and disordering the time sequences, 80% of these days were used to build the potential forecast equations and the remaining 20% were used to validate the accuracy of the equations.

Statistical model performances were evaluated according to the following factors: R^2 (variance in the individual model's coefficients of determination), RMSE (root mean square error), and CV (coefficient of variation defined as RMSE/mean MDA8 O_3). All statistics are based on MATLAB R2015b.

3. Results and discussion

3.1 Characteristics and variation trend of ozone concentrations in North China

The MDA8 O_3 concentration is one of six factors used to calculate the daily air-quality index in China. Five ranks are separated, representing different air-quality levels: excellent, good, lightly polluted, moderately polluted and heavily polluted days, with cut-off concentrations of 100, 160, 215 and 265 μg m^{-3}, respectively. The Grade II National Ambient Air Quality Standard for the daily limit is 160 μg m^{-3}. The spatial distribution of the averaged MDA8 O_3 concentration (Fig. 1b) and exceedance ratio, which represents the proportion of days exceeding the standard (160 μg m^{-3}) (Fig. 1c), as well as detailed information on the 58 cities (Table S1), show a severe ozone pollution problem during the recent five years in North China. The domain-averaged MDA8 O_3 concentration for 58 cities was 122±11 μg m^{-3}, with an increasing rate of 7.88 μg m^{-3} $year^{-1}$ and exceedance ratio of 22.2±8.2%. Notably, the most polluted cities are concentrated in Beijing, the southeast of Hebei and the west and north of Shandong, where the average MDA8 O_3 concentration was 130±9 μg m^{-3} and exceedance ratio was 27.9±7.2%.

The daily evolution of MDA8 O_3 concentrations during 2013-2017 in 14 cities (Fig. 2a) indicates periodic, consistent and regional characteristics of ozone pollution. The most highly polluted periods are from mid-May to mid-July. Especially in 2017, the frequency and level of ozone pollution increased significantly, and regionally persistent ozone pollution events increased. The rate of the MDA8 O_3 concentration increase during 2013-2017 was 0.87 μg m^{-3} $month^{-1}$ (Fig. 2b), and this growth was accompanied by a decreasing trend of the $PM_{2.5}$ concentration (Fig. S1). The reduction of the particle's extinction due to the decreased $PM_{2.5}$ concentration can lead to an increase in radiation reaching the ground; in addition, Li et al. (2019) suggested that decreased $PM_{2.5}$ slowed down the aerosol sink of hydro-peroxyl (HO_2) radicals and thus stimulated ozone production. Thus, the rise in ozone is partly due to the decline in $PM_{2.5}$. Overall, the annual domain-averaged MDA8 O_3 concentrations for 58 cities were 102, 109, 116, 119 and 136 μg m^{-3} in 2013, 2014, 2015, 2016 and 2017, respectively (Fig. 3a). The exceedance ratios for all cities were found to be 12.9%-19.4% during 2013 to 2016, but reached 31.1% in 2017.

The monthly mean MDA8 O_3 concentrations (Fig. 3b) from April-October were 112, 138, 149, 132, 124, 117 and 75 μg m^{-3}, respectively, and the corresponding exceedance ratios were 9.4, 30.1, 41.1, 26.1, 20.3 20.1 and 3.3%. The highest domain-averaged MDA8 O_3 concentration and exceedance ratio occurred in June, followed by May, July, August, September, April and October. Meteorological conditions led to high ozone concentrations in June, and monsoon circulation in July and August resulted in cloudy, rainy conditions and less radiation in the study area (Wang et al., 2009c; Tang et al., 2012). The higher ozone concentrations in April compared with those in October could be associated with strong winds, resulting in the downward transport of ozone due to the lower stratosphere folding mechanism (Stohl and Trickl, 1999; Cooper et al., 2002; Delcloo, 2008; Verstraeten et al., 2015). Notably, this conclusion is different from that of Tang et al. (2012), who reported that the concentration in July was higher than that in May in North China during 2009-2010. However, as our study shows that the domain-averaged MDA8 O_3 in May was even higher than in July, the concentrated pollution episode occurred earlier, especially in 2017. The second half of May was the most polluted period and the exceedance ratio was 46.1%, which is higher than those observed in the first half of June (39.5%), the second half of June (45.4%) and the first half of July (35.6%). The reason for this difference is probably the abnormally higher temperatures in May, especially the second half of May, during 2013-2017 and particularly in 2017 (Fig. S2). Many studies have found a strong positive correlation between ozone levels and temperature (Bloomer et al., 2009; Demuzere et al., 2009; Bloomer et al., 2010; Pusede et al., 2015).

3.2 Weather types and associated surface O_3 levels

3.2.1 The meteorological conditions and regional ozone concentrations under different predominant weather types

Based on the Lamb-Jenkinson weather typing technique, 26 circulation patterns affecting North China were identified, including two vorticity types (anticyclone, A, and cyclone, C), eight directional types (northeasterly, NE; easterly, E; southeasterly, SE; southerly, S; southwesterly, SW; westerly, W; northwesterly, NW; and northerly, N) and 16 hybrids of vorticity and directional types (CN, CNE, CE, CSE, CS, CSW, CW, CNW, AN, ANE, AE, ASE, AS, ASW, AW, and ANW). The composite mean sea level pressure maps, along with the occurrence days, are shown in Fig. 4. Obvious positional differences between the high- and low-pressure centers have been shown in different weather types and resulted in different meteorological variables. The occurrence ratios of vorticity types, pure directional types, and the hybrid types were 35.6%, 38.8% and 25.6% in all 1070 days, respectively.

The mid-latitude eastern Eurasian continent is strongly affected by monsoon circulation, and there are several key synoptic systems affecting the circulation and meteorological conditions in North China. During our study period, North cyclones (Mongolian and Yellow River cyclone), indicative of a low-pressure system located in the northwest of North China, dominate in spring and summer. The Siberian High influences northern China in spring and autumn. The Western Pacific Subtropical High is also a key system in summer. Therefore, these main synoptic systems result in frequency variations of weather types in different months over North China.

According to the different locations of the different central systems, together with the similar meteorological factors and mean MDA8 O_3 values in these circulation patterns, 26 circulation types were merged into 5 weather categories: 1) N-E-S direction (geostrophic wind direction diverts from north to south) including N, NE, E, SE, AN, ANE, AE and ASE; 2) S-W-N direction (geostrophic wind direction diverted from south to north)including S, SW, W, NW, AS, ASW, AW and ANE; 3) LP (low-pressure related weather types) including CN, CNE, CE, CSE, CS, CSW, CW and CNW; 4) A (anticyclone); and 5) C (cyclone). The occurrence ratios of 5 weather categories were 25.4%, 26.5%, 12.5%, 17.5% and 18.1% in all 1070 days, respectively. The predominant local meteorological conditions associated with a specific weather category play an important role in ozone pollution, influencing ozone photoreaction or its regional transport. The statistical values of averaged MDA8 O_3 concentration, frequency of weather types/categories and meteorological variables are depicted in Table 1 and Fig. 5. Briefly, the N-E-S direction and A categories were typically associated with cool and wet air, moderate rain and TCC, low BLH, as well as relatively clean air masses from the region of the inner-Mongolia/eastern ocean (Fig. S3), which is unfavorable for ozone formation, and the corresponding area-averaged MDA8 O_3 concentrations were 98±6 μg m^{-3} and 96 μg m^{-3}, respectively. The S-W-N direction category with moderate T and BLH, lower RH, weak wind, sporadic clouds and rain, and stronger subsidence in the lower troposphere contributed to higher ozone levels (122±8 μg m^{-3}). The highest ozone concentrations (126±16 and 128 μg m^{-3}) were related to LP and C categories, respectively, which can probably be attributed to favorable meteorological conditions (hot and humid air, a small amount of TCC and rainfall, and high BLH) for ozone formation and transport. However, CE and CSE are different from the other weather types in the LP category, with lower O_3 concentrations due to lower temperatures and easterly winds from the ocean. Overall, the peak values of ozone always occurred in the front of the cold frontal passage or cyclone (most weather types in LP and C), whereas the valley values exhibited during or after the cold frontal passage (most weather types in the N-E-S direction, C with heavy rainfall and CE); similar conclusions were also reported previously (Cooper et al., 2001; Cooper et al., 2002; Chen et al., 2008)

3.2.2 Spatial distributions of the 26 weather types/five categories

The spatial distribution of the averaged MDA8 O_3 concentration under different weather types is shown in Fig. 6, and Figs. S3-S7 display the spatial distributions of the combined wind field with BLH, maximum temperature (Tmax), RH, rain and TCC, respectively. In most cities, the lowest MDA8 O_3 concentrations occurred in the weather categories N-E-S direction and A. The S-W-N direction category, having predominantly southerly winds in the whole or south of North China, exhibited a high-value ozone along with the prevailing wind direction. The LP and C weather categories, having the highest regional averaged levels, were associated with high Tmax and strong southerly flow, moderate RH and ample sunshine, the meteorological conditions that are favorable for ozone formation as well as the transport of ozone and its precursors from the polluted area.

3.2.3 Inter-annual/monthly ozone variation elaborated from the perspective of circulation patterns changes

The inter-annual or monthly ozone concentration changes are associated with variations in weather types. Fig. 3 indicates that the ratios of high-ozone weather categories (S-W-N direction, LP and C S-W-N direction, LP and C) were most frequent in 2013 and 2017, less frequent in 2015 and 2016, and least frequent in 2014. The high-ozone weather categories accounted for 61.5% and 61.8% of the time in 2013 and 2017, respectively. In similar weather conditions, lower ozone levels could also be associated with the higher $PM_{2.5}$ levels in 2013 and 2015. Quantifying the contribution of frequency-only and circulation changes (frequency and intensity) to the inter-annual variability of ozone will be discussed in Section 3.3.

Affected by monsoon circulation systems, the frequencies of weather types vary dramatically on a monthly scale (Fig. 3b). The frequencies of both N-E-S direction and A decrease gradually in spring, whereas the frequencies of the S-W-N direction, LP and C gradually increase. In autumn, the frequencies of LP and C decrease, whereas those of S-W-N direction, N-E-S direction and A increase. The weather categories C and LP dominate in summer. The high-ozone weather categories (S-W-N direction, LP and C) accounted for 58.7, 66.5, 79.3, 80.6, 49.0, 38.0 and 27.7% of the time in the months from April to October, respectively. These frequencies were highest in July, June, and May, which probably resulted in the highest monthly averaged regional ozone concentrations. However, due to the influence of monsoon circulation in July, large amounts of rainfall occurred during this month: 73 out of 194 days during the 5 years were rainy in category C, which reduced ozone levels. Notably, severe ozone pollution in May and especially in the second half of May in 2017 is closely related to abnormally high frequency under the control of most-polluted synoptic categories (LP and C), accounting for 35.5% in 31 days and 50.0% in 16 days, respectively (Table S2). With the development of the Siberian High from August to October, the weather categories N-E-S direction and A occurred frequently and the monthly averaged ozone concentrations declined.

3.3 Effects of synoptic changes on inter-annual ozone variability

3.3.1 Effect of weather types intensity on inter-annual ozone variability

The pressure fields for 26 synoptic types per year during 2013-2017 (Figs. S8-S9) show that every synoptic weather type varies in both frequency and intensity. The intensity of circulation patterns indicates the difference of the center pressure, the location of the predominant system, the pressure gradient, and the domain-averaged sea level pressure. There were different correlations between ECII and ΔO_3 (as introduced in Section 2.4) in different circulation types for different cities. For instance, the strong negative correlation between these two variables for the weather type C in ZJK (Fig. 7a) indicates that lower values of min slp were associated with higher MDA8 O_3 concentrations.

The number of cities and averaged r according to corresponding ECII under each circulation type among 14 cities are shown in Fig. 7b. Overall, the average absolute value of r was 0.74. For the circulation type C, ΔO_3 correlated with min slp best in 9 of the cities, and the average r was -0.81, i.e., a strong negative correlation. A strong negative correlation between ΔO_3 and pressure gradient is evident for the circulation type N, whereas an opposite pattern occurs for circulation types CSE and CS. The reasons for this difference are as follows. Northerly winds are the prevailing for type N, and a high-pressure gradient indicates strong northerly winds bringing clean air mass from the north, which results in a decrease in the MDA8 O_3 concentration. However, high temperatures and RH as well as prevailing southerly or easterly winds (Figs. S3-S5) occur in southern cities in types CSE and CS. In addition, the abundance of precursors and ozone in the upwind region facilitate ozone formation and transport with the increasing pressure gradient (wind speeds).

Even under the same weather type controls, the ECII and the value of r in different cities are different. This phenomenon is caused by the differences in geographic location, topographic discrepancy, and the properties of the upwind air mass, etc. Therefore, under the control of the same weather type, the ECII of adjacent cities is the same.

3.3.2 Quantifying the effects of the inter-annual synoptic changes on the inter-annual ozone variability

Based on Equations (1) and (2), we reconstructed the inter-annual ozone levels by taking into account either frequency-only or both frequency and intensity variations of synoptic circulations, which are $\overline{\overline{O_{3m}}}(\text{fre})$ and $\overline{\overline{O_{3m}}}(\text{fre}+\text{int})$, respectively. The difference between maximum and minimum annual reconstructed ozone is labeled as $\Delta\overline{\overline{O_{3m}}}(\text{fre})$ and $\Delta\overline{\overline{O_{3m}}}(\text{fre}+\text{int})$, respectively. ΔO_3_obs is different between maximum and minimum for annual observed O_3 concentration. Thus, the contributions of inter-annual variability in O_3 influenced by frequency-only and by frequency and intensity variation of synoptic circulation are $\Delta\overline{\overline{O_{3m}}}(\text{fre})/\Delta O_3\_\text{obs}$ and $\Delta\overline{\overline{O_{3m}}}(\text{fre}+\text{int})/\Delta O_3\_\text{obs}$, respectively, which indicates the inter-annual ozone levels oscillation caused by synoptic variability.

The observed and reconstructed (influenced by frequency-only and by frequency and intensity variations of synoptic circulations) inter-annual MDA8 O_3 levels for 5 years in 14 cities and the whole region are shown in Fig. 8. The contribution of inter-annual variability in O_3 influenced by frequency and intensity variation of synoptic circulation ranged from 44.1 to 69.8% over the 14 cities, and the contribution by the frequency-only variation ranged from 5.2 to 23.4%. Obviously, the inter-annual fluctuation of the ozone concentration is caused mainly by weather type intensity changes in North China. In addition, based on regional averaged scale, inter-annual variability in domain-averaged observed MDA8 O_3 in 14 cities varied from averaged maximum values 135 μg m^{-3} in 2017 to a minimum 104 μg m^{-3} in 2013. The contributions of variations in circulation patterns to inter-annual O_3 increase was 39.2%, and the remaining inter-annual variability was possibly due to nonlinear relationships with recent emission control measures over North China.

Our results (44.1-69.8%) are higher than that (50%) of Zhang et al. (2013) in most cities. The difference could be attributed to our results being based on (1) more weather types; (2) weather types covering all days; (3) more CIIs, which can better characterize intensity. Furthermore, a higher contribution in single city and increasing reconstructed ozone indicate that synoptic circulation patterns play an important role in ozone variability in North China. However, our regional result (39.2%) is lower than that (46%) of Hegarty et al. (2007), which reveals that the increasing trend for ozone from 2013 to 2017 in North China is associated with the impact of its precursors to a large extent.

3.4 Quantifying the impact of weather patterns on day-to-day ozone concentration and forecasting daily ozone concentration

Based on the five weather categories defined in Section 3.2.1, a segmented synoptic-regression analysis approach (introduced in Section 2.5) was established to quantify the impact of weather patterns on day-to-day ozone concentration and construct the ozone potential forecast model.

The contribution of local meteorological factors to the day-to-day variation of ozone can be evaluated by the explained variance (R_E^2) calculated from the synoptic-regression-based models (Hien et al., 2002; Wang et al., 2009b). Overall, the predicted versus observed MDA8 O_3 concentrations of the validation data are shown in Fig. 9; the predicted concentrations were obtained by inputting the validation data (the part that did not build the model was 20% of the total data) into the corresponding model equations of five weather categories for each city. Local meteorological parameters could explain 57-63% and 41-52% of the day-to-day MDA8 O_3 concentration variability for the northern cities (except for QHD, 34%) and southern cities (except for ZZ, 20%), respectively.

In addition, the results of segmented synoptic-regression analysis in 14 cities, i.e., the daily MDA8 O_3 potential forecast equations for each category in each city, are shown in Table S3. Table 2 represents the number of cities (in total 14) from which the meteorological factors were used in a stepwise regression model under each weather category. The results show that Tmax shows a strongly positively correlation with ozone, being the primary influencing factor in all categories and all cities, as high temperatures are related to large ozone concentrations in North China. V shows a positive correlation with O_3 in the northern part of this region (approximately 38.5°N as the north-south boundary), which means that the southerly flow causes an increase in ozone concentration. Therefore, as discussed in Section 3.2.2, high temperatures and southerly winds are the main factors contributing to increased ozone concentrations in North China from a regional perspective. Both RH_lag and RH show a negative correlation with O_3, and the former has more occurrences and weight in equations. The phenomenon may exist because an RH of approximately 40-50% (Zhao et al., 2019) generates more hydroxyl radicals (OH) facilitating ozone formation, and ozone is stored in the residual layer and is transported into the surface during the next day by convection and diffusion. In addition, TCC is a key factor.

Three statistical measures (R^2, RMSE, and CV) for building and validation datasets for the 5 weather categories and the composite model, which integrates the 5 weather categories, in 14 cities (Table S4) indicated that the potential forecast equations of MDA8 O_3 in most cities are acceptable. Scatter plots of predicted versus observed MDA8 O_3 concentrations in composite validation datasets in each city are shown in Fig. 9. For validation data, the prediction of ozone concentration was obtained by inputting the meteorological factors into the corresponding weather category's simulated formula of a specific city; therefore, composite validation datasets indicate that the prediction ozone concentration of five categories are integrated. The result of validation shows that R^2 was higher than 0.50 except for QHD, SJZ and ZZ (0.24-0.47), while CV was lower than 40% except for TY and ZZ.

The results reveal that most of the validation data are within the acceptable error range within the 2:1 and 1:2 ratio lines, and the scatters are distributed evenly around the 1:1 line. For example, the comparison of the observed and predicted ozone in Beijing during our study period is shown in Fig. S10. This finding also indicates that the segmented synoptic-regression approach is practicable to construct the ozone potential forecasting model in most cities in North China.

In brief, the aforementioned results can provide references for daily MDA8 O_3 prediction for each city and facilitate understanding and evaluating the impact of local meteorology on daily ozone variation on an urban scale.

4 Conclusions

In this study, we demonstrated inter-annual/monthly variation in the surface MDA8 O_3 concentration in North China during April-October 2013-2017, investigated the relationship between weather types and MDA8 O_3 levels, quantified the contribution of weather types and local variations in meteorological factors on both inter-annual and day-to-day variability of ozone, and built the ozone potential forecast equations. The main results are as follows:

1. The annual domain-averaged concentrations of MDA8 O_3 during 2013-2017 were 102, 109, 116, 119, and 136 μg m^{-3}, respectively, and the highest exceedance ratio (31.1%) was observed in 2017. The monthly mean MDA8 O_3 concentrations were 112, 138, 149, 132, 124, 117, and 75 μg m^{-3} in April to October, respectively, with a significantly increasing rate of 0.87 μg m^{-3} $month^{-1}$ during the five-year period. The most polluted cities are concentrated in Beijing, the southeast of Hebei and the west and north of Shandong.

2. Twenty-six weather types were objectively identified based on the Lamb-Jenkinson method and combined into five weather categories due to similar meteorological factors and MDA8 O_3 concentrations. The high ozone levels in 2017, and during May-July, were partly due to the high frequency of the highly polluted weather categories (S-W-N direction, LP and C) due to high temperatures, moderate RH and southerly air flows.

3. Intensity of synoptic circulation patterns is the dominant factor through which variations in weather types influence the variability of ozone levels. The contribution of inter-annual variability in O_3 influenced by both frequency and intensity variations of synoptic circulation patterns ranged from 44 to 70% over the 14 cities considered in detail, whereas the contributions of variations in circulation patterns to the inter-annual O_3 increase from 2013 to 2017 was only 39.2% based on a regionally averaged scale.

4. The results of daily ozone potential forecast equations in the 14 cities show that high temperatures, moderate RH and southerly winds could result in severe ozone pollution in the northern part of North China, whereas the southern part is affected mainly by high temperatures and RH. Local meteorological parameters could explain 55-64% and 43-49% of the day-to-day MDA8 O_3 variability for the northern cities (except for QHD, 32%) and southern cities (except for ZZ, 25%), respectively.

Author contribution

LL Wang designed this research. JD Liu and LL Wang interpreted the data and wrote the paper. MG Li processed some of the data. The weather type classification program was provided by ZH Liao. Y Sun, T Song, and WK Gao provided some of the $PM_{2.5}$ and O_3 data. Y Li provided some of the meteorological data. All of the authors commented on the paper.

Data availability

Daily average mass concentrations of ozone were obtained from the National Urban Air Quality Real-time Publishing Platform (http://106.37.208.233:20035/) issued by the Chinese Ministry of Ecology and Environment. Daily meteorological data were obtained from the China Meteorological Administration in the Meteorological Information Combine Analysis and Process System (MICAPS), and daily meteorological reanalysis data (gridded at 1°× 1°) were obtained from ERA-Interim (https://apps.ecmwf.int/datasets/data/interim-full-daily/levtype=sfc/). All of the data can be obtained upon request.

Competing interests

The authors declare that they have no conflict of interest.

Acknowledgments

This work was partially supported by grants from the National Key R&D Plan (Quantitative Relationship and Regulation Principle between Regional Oxidation Capacity of Atmospheric and Air Quality 2017YFC0210003), the National Natural Science Foundation of China (No. 41505133 & 41775162), the Strategic Priority Research Program of the Chinese Academy of Sciences (No. XDA19020303), the National Research Program for Key Issues in Air Pollution Control (DQGG0101) and a program of the China Scholarships Council. We give special thanks to the National Earth System Science, Data Sharing Infrastructure, and the National Science & Technology Infrastructure of China.

References

Barrero, M. A., Grimalt, J. O., and Cantón, L.: Prediction of daily ozone concentration maxima in the urban atmosphere, Chemometrics and Intelligent Laboratory Systems, 80, 67-76, 10.1016/j.chemolab.2005.07.003, 2006.

Bloomer, B. J., Stehr, J. W., Piety, C. A., Salawitch, R. J., and Dickerson, R. R.: Observed relationships of ozone air pollution with temperature and emissions, Geophysical Research Letters, 36, 269-277, 2009.

Bloomer, B. J., Vinnikov, K. Y., and Dickerson, R. R.: Changes in seasonal and diurnal cycles of ozone and temperature in the eastern U.S, Atmospheric Environment, 44, 2543-2551, 2010.

Chan, C. K., and Yao, X.: Air pollution in mega cities in China, Atmospheric Environment, 42, 1-42, 10.1016/j.atmosenv.2007.09.003, 2008.

Chen, Z. H., Cheng, S. Y., Li, J. B., Guo, X. R., Wang, W. H., and Chen, D. S.: Relationship between atmospheric pollution processes and synoptic pressure patterns in northern China, Atmospheric Environment, 42, 6078-6087, 10.1016/j.atmosenv.2008.03.043, 2008.

Comrie, A. C., and Yarnal, B.: Relationships between synoptic-scale atmospheric circulation and ozone concentrations in Metropolitan Pittsburgh, Pennsylvania, Atmospheric Environment.part B.urban Atmosphere, 26, 301-312, 1992.

Conway, D., and Jones, P. D.: The use of weather types and air flow indices for GCM downscaling, Journal of Hydrology, 212-213, 348-361, https://doi.org/10.1016/S0022-1694(98)00216-9, 1998.

Cooper, O. R., Moody, J. L., Parrish, D. D., Trainer, M., Ryerson, T. B., Holloway, J. S., Hübler, G., Fehsenfeld, F. C., Oltmans, S. J., and Evans, M. J.: Trace gas signatures of the airstreams within North Atlantic cyclones: Case studies from the North Atlantic Regional Experiment (NARE ’97) aircraft intensive, Journal of Geophysical Research: Atmospheres, 106, 5437-5456, 10.1029/2000jd900574, 2001.

Cooper, O. R., Moody, J. L., Parrish, D. D., Trainer, M., Holloway, J. S., Hübler, G., Fehsenfeld, F. C., and Stohl, A.: Trace gas composition of midlatitude cyclones over the western North Atlantic Ocean: A seasonal comparison of O3 and CO, Journal of Geophysical Research: Atmospheres, 107, ACH 2-1-ACH 2-12, 10.1029/2001jd000902, 2002.

Delcloo, A. W. a. D. B., H.: Five day 3D back trajectory clusters and trends analysis of the Uccle ozone sounding time series in the lower troposphere (1969–2001), Atmos. Environ., 42, 4419–4432, 2008.

Demuzere, M., Trigo, R. M., Vila-Guerau de Arellano, J., and van Lipzig, N. P. M.: The impact of weather and atmospheric circulation on O3 and PM10 levels at a rural mid-latitude site, Atmos. Chem. Phys., 9, 2695-2714, https://doi.org/10.5194/acp-9-2695-2009, 2009.

Demuzere, M., and van Lipzig, N. P. M.: A new method to estimate air-quality levels using a synoptic-regression approach. Part I: Present-day O3 and PM10 analysis, Atmospheric Environment, 44, 1341-1355, https://doi.org/10.1016/j.atmosenv.2009.06.029, 2010.

Eder, B. K., Davis, J. M., and Bloomfield, P.: An Automated Classification Scheme Designed to Better Elucidate the Dependence of Ozone on Meteorology, J.appl.meteor, 33, 1182-1199, 1994.

Fleming, Z. L., Doherty, R. M., Von Schneidemesser, E., Malley, C. S., Cooper, O. R., Pinto, J. P., Colette, A., Xu, X., Simpson, D., Schultz, M. G., Lefohn, A. S., Hamad, S., Moolla, R., Solberg, S., and Feng, Z.: Tropospheric Ozone Assessment Report: Present-day ozone distribution and trends relevant to human health, Elem Sci Anth, 6, 12, 10.1525/elementa.273, 2018.

He, J., Yu, Y., Xie, Y., Mao, H., Wu, L., Liu, N., and Zhao, S.: Numerical Model-Based Artificial Neural Network Model and Its Application for Quantifying Impact Factors of Urban Air Quality, Water, Air, & Soil Pollution, 227, 10.1007/s11270-016-2930-z, 2016.

He, J., Gong, S., Yu, Y., Yu, L., Wu, L., Mao, H., Song, C., Zhao, S., Liu, H., Li, X., and Li, R.: Air pollution characteristics and their relation to meteorological conditions during 2014-2015 in major Chinese cities, Environmental pollution, 223, 484-496, 10.1016/j.envpol.2017.01.050, 2017.

Hegarty, J., Mao, H., and Talbot, R.: Synoptic controls on summertime surface ozone in the northeastern United States, Journal of Geophysical Research, 112, 10.1029/2006jd008170, 2007.

Hien, P. D., Bac, V. T., Tham, H. C., Nhan, D. D., and Vinh, L. D.: Influence of meteorological conditions on PM2.5 and PM2.5-10 concentrations during the monsoon season in Hanoi, Vietnam, Atmospheric Environment, 36, 3473-3484, 10.1016/s1352-2310(02)00295-9, 2002.

Jacob, D. J., and Winner, D. A.: Effect of climate change on air quality, Atmospheric Environment, 43, 51-63, 10.1016/j.atmosenv.2008.09.051, 2009.

Kinney, P. L.: Climate change, air quality, and human health, American journal of preventive medicine, 35, 459-467, 10.1016/j.amepre.2008.08.025, 2008.

Lamb, H.: British Isles weather types and a register of the daily sequence of circulation patterns, Geophys. Mem, 116, 1861-1971, 1972.

Li, K., Jacob, D. J., Liao, H., Shen, L., Zhang, Q., and Bates, K. H.: Anthropogenic drivers of 2013–2017 trends in summer surface ozone in China, Proceedings of the National Academy of Sciences, 116, 422-427, 10.1073/pnas.1812168116, 2019.

Liao, Z., Gao, M., Sun, J., and Fan, S.: The impact of synoptic circulation on air quality and pollution-related human health in the Yangtze River Delta region, The Science of the total environment, 607-608, 838-846, 10.1016/j.scitotenv.2017.07.031, 2017.

Liu, Y., Franklin, M., Kahn, R., and Koutrakis, P.: Using aerosol optical thickness to predict ground-level PM2.5 concentrations in the St. Louis area: A comparison between MISR and MODIS, Remote Sens. Environ., 107, 33-44, 10.1016/j.rse.2006.05.022, 2007.

Liu, Y., He, K. B., Li, S. S., Wang, Z. X., Christiani, D. C., and Koutrakis, P.: A statistical model to evaluate the effectiveness of PM2.5 emissions control during the Beijing 2008 Olympic Games, Environ. Int., 44, 100-105, 10.1016/j.envint.2012.02.003, 2012.

Lu, X., Hong, J., Zhang, L., Cooper, O. R., and Zhang, Y.: Severe Surface Ozone Pollution in China: A Global Perspective, Environmental Science & Technology Letters, 5, acs.estlett.8b00366-, 2018.

Lu, X., Zhang, L., Chen, Y., Zhou, M., Zheng, B., Ke, L., Liu, Y., Lin, J., Fu, T.-M., and Zhang, Q.: Exploring 2016–2017 surface ozone pollution over China: source contributions and meteorological influences, Atmospheric Chemistry and Physics, 19, 8339-8361, 10.5194/acp-19-8339-2019, 2019.

Mckendry, I. G., Stahl, K., and Moore, R. D.: Synoptic sea-level pressure patterns generated by a general circulation model: comparison with types derived from NCEP/NCAR re-analysis and implications for downscaling, International Journal of Climatology, 26, 1727-1736, 2006.

Mills, G., Pleijel, H., Malley, C. S., Sinha, B., Cooper, O. R., Schultz, M. G., Neufeld, H. S., Simpson, D., Sharps, K., Feng, Z., Gerosa, G., Harmens, H., Kobayashi, K., Saxena, P., Paoletti, E., Sinha, V., and Xu, X.: Tropospheric Ozone Assessment Report: Present-day tropospheric ozone distribution and trends relevant to vegetation, Elem Sci Anth, 6, 47, 10.1525/elementa.302, 2018.

Monks, P. S., Granier, C., Fuzzi, S., Stohl, A., Williams, M. L., Akimoto, H., Amann, M., Baklanov, A., Baltensperger, U., Bey, I., Blake, N., Blake, R. S., Carslaw, K., Cooper, O. R., Dentener, F., Fowler, D., Fragkou, E., Frost, G. J., Generoso, S., Ginoux, P., Grewe, V., Guenther, A., Hansson, H. C., Henne, S., Hjorth, J., Hofzumahaus, A., Huntrieser, H., Isaksen, I. S. A., Jenkin, M. E., Kaiser, J., Kanakidou, M., Klimont, Z., Kulmala, M., Laj, P., Lawrence, M. G., Lee, J. D., Liousse, C., Maione, M., McFiggans, G., Metzger, A., Mieville, A., Moussiopoulos, N., Orlando, J. J., O'Dowd, C. D., Palmer, P. I., Parrish, D. D., Petzold, A., Platt, U., Pöschl, U., Prévôt, A. S. H., Reeves, C. E., Reimann, S., Rudich, Y., Sellegri, K., Steinbrecher, R., Simpson, D., ten Brink, H., Theloke, J., van der Werf, G. R., Vautard, R., Vestreng, V., Vlachokostas, C., and von Glasow, R.: Atmospheric composition change – global and regional air quality, Atmospheric Environment, 43, 5268-5350, https://doi.org/10.1016/j.atmosenv.2009.08.021, 2009.

Monks, P. S., Archibald, A. T., Colette, A., Cooper, O., Coyle, M., Derwent, R., Fowler, D., Granier, C., Law, K. S., Mills, G. E., Stevenson, D. S., Tarasova, O., Thouret, V., Schneidemesser, E. v., Sommariva, R., Wild, O., and Williams, M. L.: Tropospheric ozone and its precursors from the urban to the global scale from air quality to short-lived climate forcer, Atmospheric Chemistry and Physics, 15, 8889-8973, 10.5194/acp-15-8889-2015, 2015.

Moody, J. L., Munger, J. W., Goldstein, A. H., Jacob, D. J., and Wofsy, S. C.: Harvard Forest regional-scale air mass composition by Patterns in Atmospheric Transport History (PATH), Journal of Geophysical Research: Atmospheres, 103, 13181-13194, 10.1029/98jd00526, 1998.

Pope, R. J., Butt, E. W., Chipperfield, M. P., Doherty, R. M., Fenech, S., Schmidt, A., Arnold, S. R., and Savage, N. H.: The impact of synoptic weather on UK surface ozone and implications for premature mortality, Environmental Research Letters, 11, 124004, 10.1088/1748-9326/11/12/124004, 2016.

Pusede, S. E., Steiner, A. L., and Cohen, R. C.: Temperature and Recent Trends in the Chemistry of Continental Surface Ozone, Chemical Reviews, 115, 3898-3918, 10.1021/cr5006815, 2015.

Robeson, S. M., and Steyn, D. G.: Evaluation and comparison of statistical forecast models for daily maximum ozone concentrations, Atmospheric Environment Part B Urban Atmosphere, 24, 303-312, 1990.

Russo, A., Trigo, R. M., Martins, H., and Mendes, M. T.: NO2, PM10 and O3 urban concentrations and its association with circulation weather types in Portugal, Atmospheric Environment, 89, 768-785, 10.1016/j.atmosenv.2014.02.010, 2014.

Santurtún, A., González-Hidalgo, J. C., Sanchez-Lorenzo, A., and Zarrabeitia, M. T.: Surface ozone concentration trends and its relationship with weather types in Spain (2001–2010), Atmospheric Environment, 101, 10-22, 2015.

Shen, L., Mickley, L. J., and Tai, A. P. K.: Influence of synoptic patterns on surface ozone variability over the eastern United States from 1980 to 2012, Atmospheric Chemistry and Physics, 15, 10925-10938, 10.5194/acp-15-10925-2015, 2015.

Stohl, A., and Trickl, T.: A textbook example of long-range transport: Simultaneous observation of ozone maxima of stratospheric and North American origin in the free troposphere over Europe, Journal of Geophysical Research Atmospheres, 104, 30445-30462, 1999.

Tang, G., Wang, Y., Li, X., Ji, D., Hsu, S., and Gao, X.: Spatial-temporal variations in surface ozone in Northern China as observed during 2009–2010 and possible implications for future air quality control strategies, Atmospheric Chemistry and Physics, 12, 2757-2776, 10.5194/acp-12-2757-2012, 2012.

Trigo, R. M., and Dacamara, C. C.: Circulation weather types and their influence on the precipitation regime in Portugal, International Journal of Climatology, 20, 1559-1581, 2000.

Verstraeten, W. W., Neu, J. L., Williams, J. E., Bowman, K. W., Worden, J. R., and Boersma, K. F.: Rapid increases in tropospheric ozone production and export from China, Nature Geoscience, 8, 690, 10.1038/ngeo2493, 2015.

Wang, T., Wei, X., Ding, A., Poon, S. C., Lam, K., Li, Y., Chan, L., and Anson, M.: Increasing surface ozone concentrations in the background atmosphere of Southern China, 1994-2007, Atmospheric Chemistry and Physics, 2009a.

Wang, W. T., Primbs, T., Tao, S., and Simonich, S. L. M.: Atmospheric Particulate Matter Pollution during the 2008 Beijing Olympics, Environmental Science & Technology, 43, 5314-5320, 10.1021/es9007504, 2009b.

Wang, Y., Hao, J., McElroy, M. B., Munger, J. W., Ma, H., Chen, D., and Nielsen, C. P.: Ozone air quality during the 2008 Beijing Olympics: effectiveness of emission restrictions, Atmospheric Chemistry and Physics, 9, 5237-5251, DOI 10.5194/acp-9-5237-2009, 2009c.

Yarnal, B.: Synoptic Climatology in Environmental Analysis A Primer, Journal of Preventive Medicine Information, 347, 170-180, 1993.

Zhang, J. P., Zhu, T., Zhang, Q. H., Li, C. C., Shu, H. L., Ying, Y., Dai, Z. P., Wang, X., Liu, X. Y., Liang, A. M., Shen, H. X., and Yi, B. Q.: The impact of circulation patterns on regional transport pathways and air quality over Beijing and its surroundings, Atmospheric Chemistry and Physics, 12, 5031-5053, 10.5194/acp-12-5031-2012, 2012.

Zhang, Y., Mao, H., Ding, A., Zhou, D., and Fu, C.: Impact of synoptic weather patterns on spatio-temporal variation in surface O3 levels in Hong Kong during 1999–2011, Atmospheric Environment, 73, 41-50, 10.1016/j.atmosenv.2013.02.047, 2013.

Zhao, W., Tang, G., Yu, H., Yang, Y., Wang, Y., Wang, L., An, J., Gao, W., Hu, B., Cheng, M., An, X., Li, X., and Wang, Y.: Evolution of boundary layer ozone in Shijiazhuang, a suburban site on the North China Plain, Journal of Environmental Sciences, 83, 152-160, https://doi.org/10.1016/j.jes.2019.02.016, 2019.

Tables

Table 1. Weather types, ozone concentrations and meteorological conditions for 5 weather categories.

category	type	ozone	fre	Tmax	RH	rain	TCC	ws	BLH	div	v-v	characteristics
N-E-S direction	N	108	5.4	25.9	64.5	2.2	6	2.1	749	0.85	2.28	MDA8 O_3 (98±6 μg m^{-3}). Cool, moderate rain, moderate TCC, and low BLH, predominant wind directions are north and east, clean air masses from inner Mongolia or the eastern ocean.
	NE	94	6.4	25.5	72.1	5.0	7	2.2	637	-1.01	-0.70	
	E	98	4.7	25.4	70.5	3.4	6	2.1	618	-1.34	-1.85	
	SE	105	2.3	22.8	71.5	4.9	7	2.4	612	-1.25	-3.85	
	AN	101	1.7	22.2	61.2	1.5	5	2.3	738	2.36	5.12	
	ANE	88	2.4	23.1	67.9	2.3	6	2.2	681	0.79	1.53	
	AE	94	1.3	23.2	65.8	2.2	7	2.3	618	-0.10	0.12	
	ASE	99	1.1	22.4	71.3	2.3	7	2.2	578	1.10	0.03	
S-W-N direction	S	112	4.1	25.4	65.7	2.2	6	2.2	642	0.28	-1.23	MDA8 O_3 (122±8 μg m^{-3}). Moderate T and BLH, lower RH, weak wind, sporadic clouds and precipitation, divergence in low troposphere. Prevailing southerly and westerly winds.
	SW	131	6.2	26.5	60.3	0.6	5	2.1	716	1.81	1.34	
	W	133	5.4	26.6	58.3	1.0	5	2.2	763	2.33	2.43	
	NW	124	4.2	26.8	58.7	1.6	6	2.3	835	1.66	3.45	
	AS	120	1.4	24.8	63.3	0.7	6	2.0	641	1.76	0.54	
	AS	114	2.6	24.5	62.2	0.7	6	1.9	666	2.53	1.02	
	AW	126	1.0	23.8	58.5	0.2	5	1.8	685	3.14	4.16	
	AN	115	1.5	23.4	55.2	0.9	6	2.3	794	2.47	5.07	
LP	CN	135	2.0	29.8	68.0	2.2	6	1.9	732	0.09	0.92	The hybrid of cyclone and direction types, MDA8 O_3 (126±16 μg m^{-3}). Widespread hot, humid, a small amount of clouds and rain, comparatively high BLH.
	CNE	119	1.8	28.2	66.0	3.2	6	2.2	724	-1.15	-0.19	
	CE	109	0.8	25.4	73.6	6.4	7	2.1	559	-2.67	-3.65	
	CSE	103	0.7	25.1	62.6	1.4	6	2.6	725	-1.65	-0.58	
	CS	123	1.0	27.4	65.7	1.6	5	2.1	693	-0.40	-0.67	
	CS	155	2.2	29.4	62.6	1.2	5	2.3	796	0.96	0.58	
	CW	140	2.6	28.6	62.3	1.3	5	2.2	778	0.95	0.93	
	CN	124	1.5	29.2	62.4	4.5	6	2.5	853	0.12	1.26	
C		128	18.1	29.5	67.1	3.8	6	2.2	715	-1.20	-1.22	Cyclone, similar to LP.
A		96	17.5	22.3	64.5	1.5	6	2.0	632	2.54	2.66	Anticyclone, similar to N-E-S direction.

Note: Ozone, MDA8 O_3 concentration (μg m^{-3}); fre, frequency of each type (%); Tmax, daily maximum temperature (℃); RH, relative humidity (%); rain, total daily precipitation (mm); TCC, total cloud cover; WS, wind speed (m s^{-1}); BLH, boundary layer height (m); div, divergence of the wind field (10^{-6} s^{-1}) from 1000 to 850 hPa (7 levels); and v-v, vertical velocity from 1000 to 100 hPa (10^{-2} Pa s^{-1}).

Table 2 All parameters used in the stepwise regression and the number of cities (out of 14) for which each variable was selected for each weather category.

factors	N-E-S direction	S-W-N direction	LP	C	A
RH (%)	2	4	3	4	6
Tmax (°C)	14	14	14	14	14
rain (mm)	0	2	2	0	2
U	2	3	3	3	1
V	9	6	6	7	2
wd (°)	2	0	0	1	1
ws (m s^{-1})	4	1	1	0	2
pre (hPa)	0	0	0	0	0
RH_lag (%)	11	5	5	4	4
Tmax_lag (°C)	3	0	0	1	0
rain_lag(mm)	1	0	0	0	0
U_lag	2	1	1	1	1
V_lag	4	0	0	0	4
wd_lag (°)	0	0	0	0	0
ws_lag (m s^{-1})	1	3	3	1	4
pre_lag (hPa)	1	0	0	1	1

Note: RH, Tmax, rain, U, V, wd, ws and pre are relative humidity, maximum temperature, precipitation, u component, v component, wind direction, wind speed and pressure, respectively. The suffix 'lag' means the meteorological factors from the previous day.

Figures

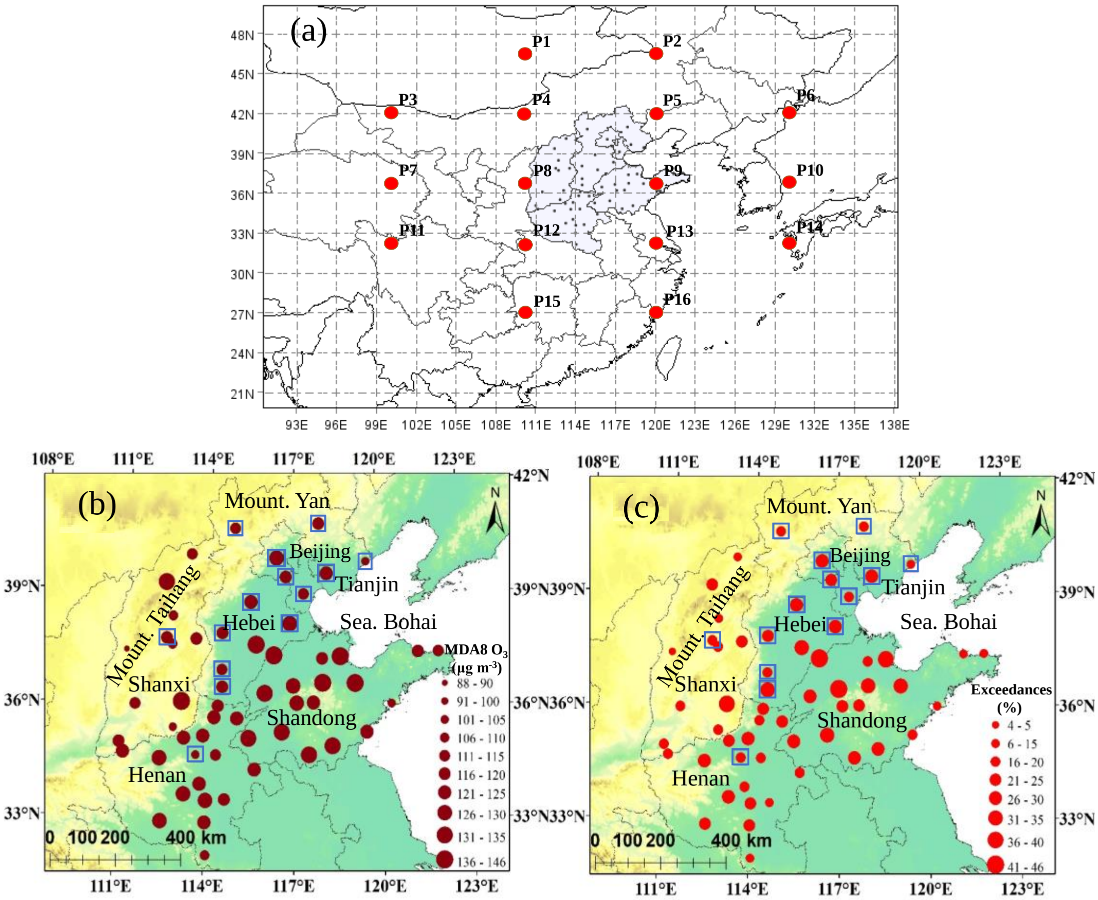

Fig. 1. Location of North China (shaded area), all cities (black spots) and sea level pressure grids (a). The 16 red points show the locations of the 5°×10° mean sea level pressure grids used for the Lamb-Jenkinson weather type classification. The spatial distributions of the maximum daily 8-h running average O_3 (MDA8 O_3) concentration (b) and exceedance ratios (c) for 58 cities. Statistics for 2013-2017 are shown with blue boxes; the other boxes are those for 2015-2017. The base map is topography; the elevations of the Taihang Mountains are more than 1200 meters, and the Yan Mountains range from 600 to 1500 meters.

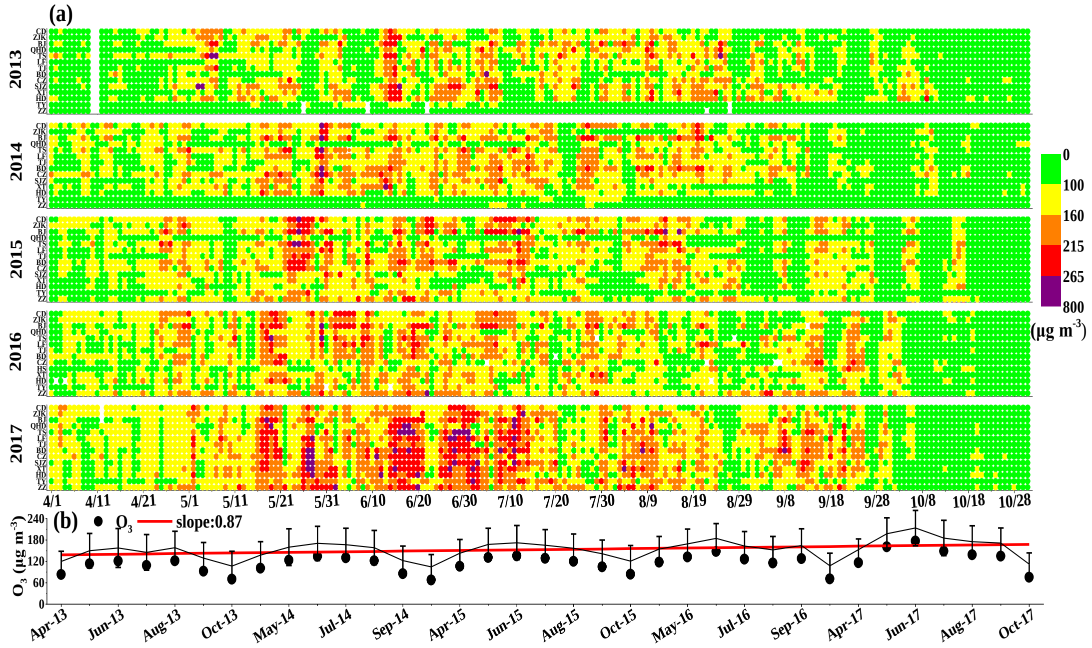

Fig. 2. Time series of daily MDA8 O_3 concentrations in 14 cities (north to south) (a), together with monthly averaged concentrations and standard deviations (b), during April to October from 2013 to 2017. Five ranks represent different air-quality levels, including excellent (green spots), good (yellow), lightly polluted (orange), moderately polluted (red) and heavily polluted (purple) days with cut-off concentrations of 100, 160, 215, and 265 μg m^{-3}, respectively. The fit line (red line) in (b) represents the increasing trend of monthly mean MDA8 O_3.

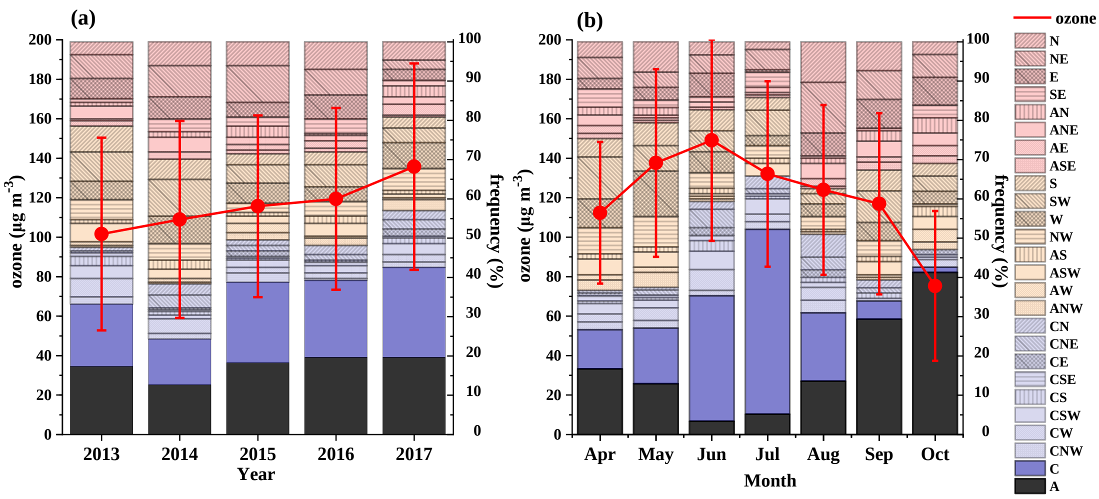

Fig. 3. Interannual (a) and monthly (b) averaged concentrations of ozone and frequencies of 26 weather types from April-October 2013-2017. The red dots represent the mean values, the vertical red lines indicate the standard deviations, and stacked charts represent the percentages of various weather types (2013 and 2014 are averaged for 14 cities; 2015-2017 are averaged for 58 cities). The pink, orange, light blue, dark blue and black areas represent the weather categories N-E-S direction, S-W-N direction, LP, C and A, respectively.

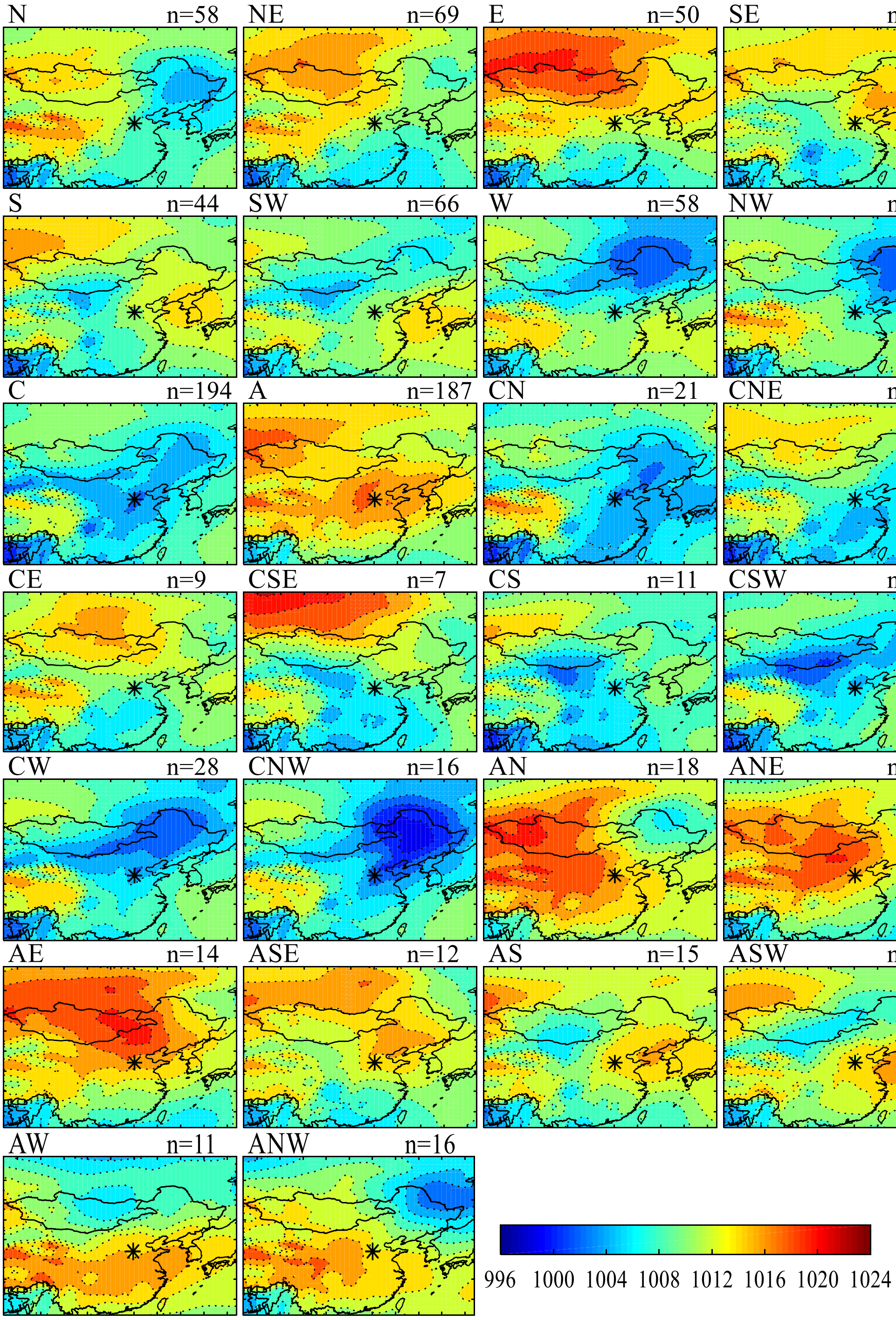

Fig. 4. Mean surface pressure field (unit: hPa) for the 26 weather types during April-October of 2013-2017 and occurrence days (1070 days in total). '*' indicates the center of North China.

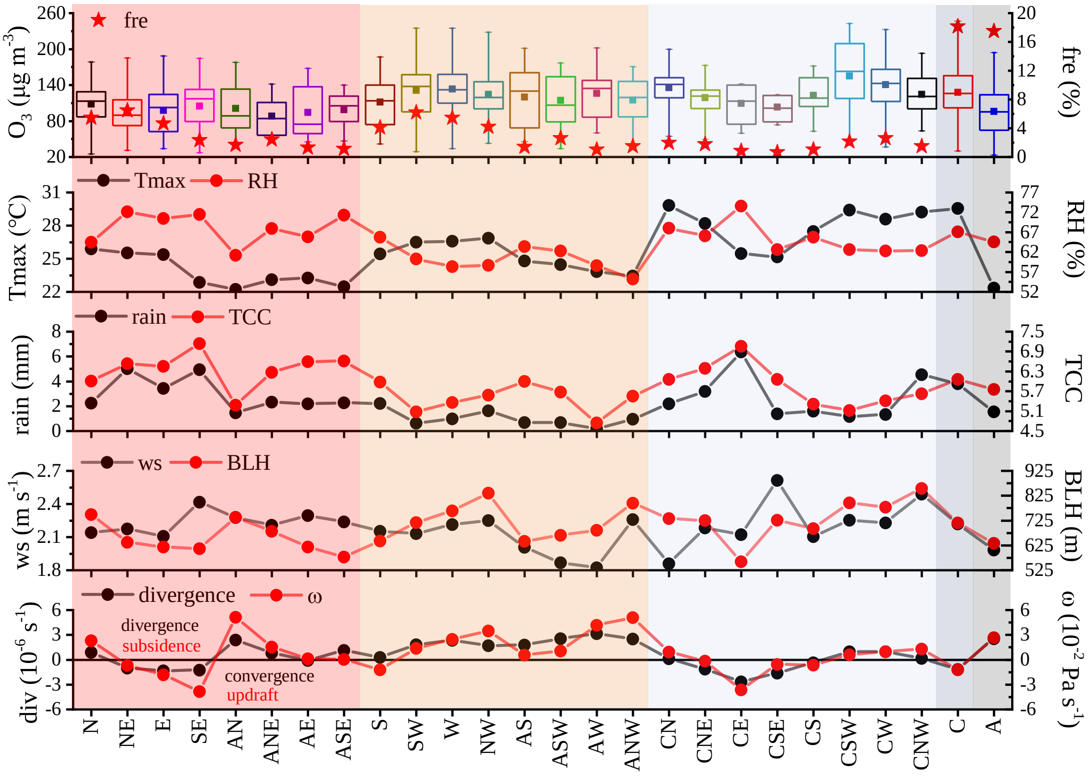

Fig. 5. Box chart of domain-averaged MDA8 O_3 concentrations, occurrence frequency of weather types (fre), and mean values of meteorological factors in 26 weather types during April-October of 2013-2017. In the box chart; the solid square indicates the mean, the horizontal lines across the box are the averages of the first, median, and the third quartiles, respectively; and the lower and upper whiskers represent the 5th and 95th percentiles, respectively. The pink, orange, light blue, dark blue and black areas represent the weather categories N-E-S direction, S-W-N direction, LP (low-pressure related weather patterns), C (cyclone) and A (anticyclone), respectively.

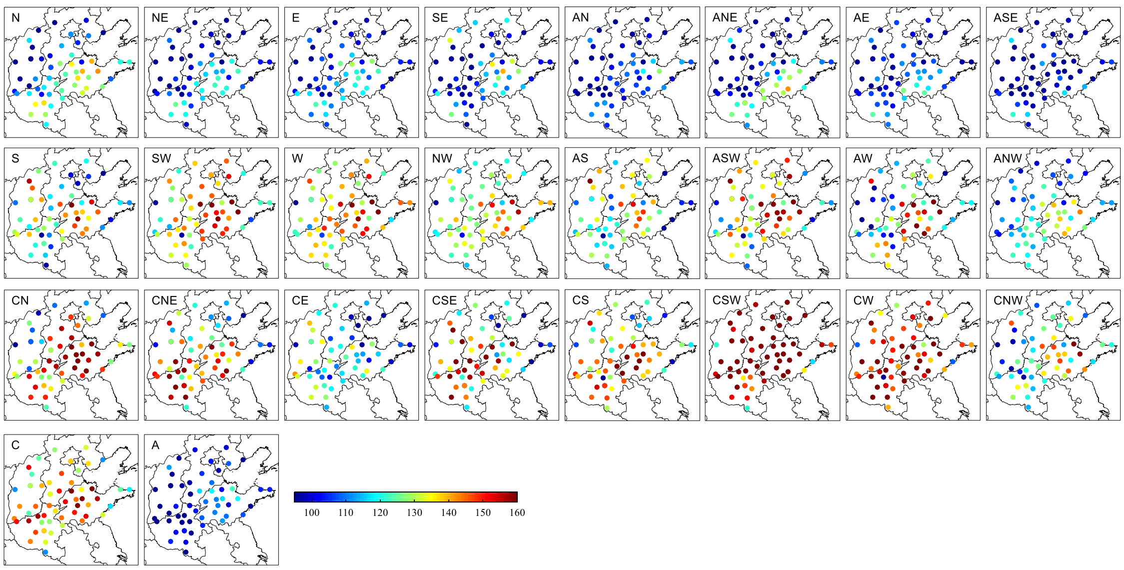

Fig. 6. Spatial distribution of average MDA8 O_3 for the 26 weather types. The first, second, and third rows correspond to the weather categories N-E-S direction, S-W-N direction and LP, respectively, and the fourth row includes both categories C and A.

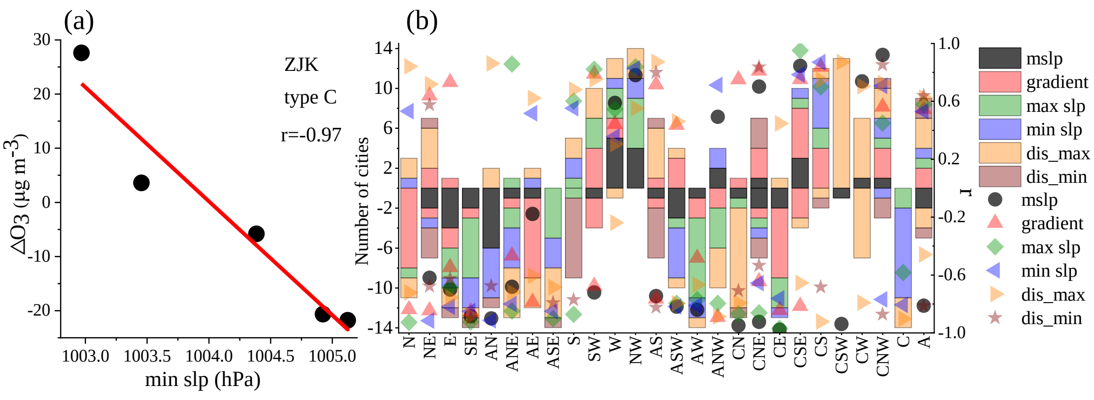

Fig. 7. Scatter plot of ΔO_3 versus min slp for weather type C in ZJK (a). The red line represents the linear fitting between min slp (the ECII under weather type C in ZJK) and ΔO_3 (the difference between the MDA8 O_3 for a given year and the corresponding 5-year average); r represents correlation coefficient. The number of cities (histogram) and averaged correlation coefficient r (points of different shapes) according to corresponding ECII under each weather type among 14 cities (b). The number of cities with positive/negative values represents positive/negative correlations between ECII and ΔO_3. For example, under CW controls, there are 1, 6 and 7 cities where ECII corresponds to mslp with the positive correlation, dis max with the positive correlation, and dis max with negative correlation, respectively, and the average r is 0.74 and 0.70, and -0.79, respectively.

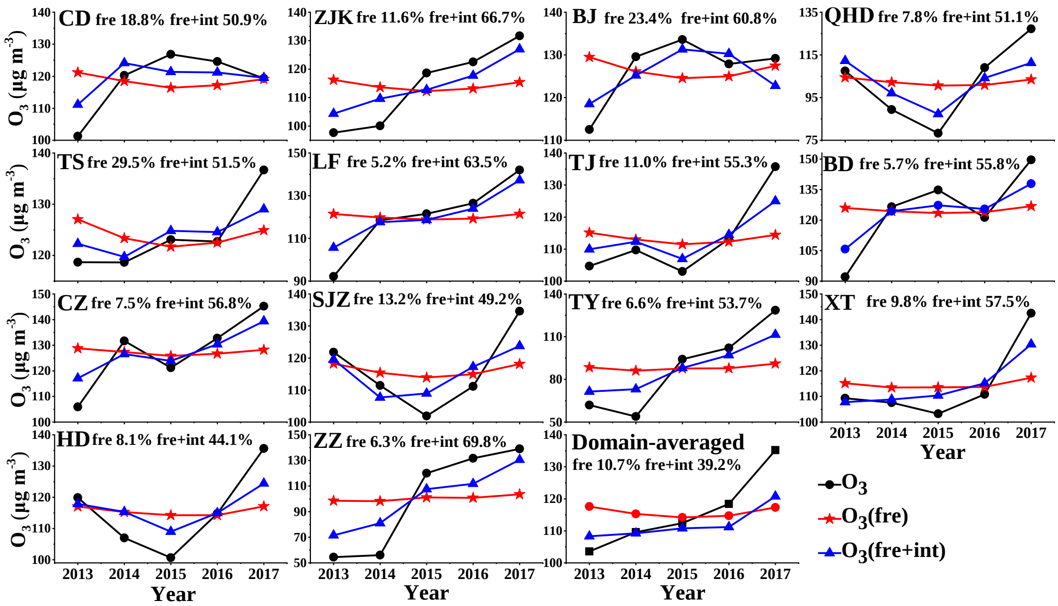

Fig. 8. The inter-annual MDA8 O_3 concentration trends for observed and the reconstructed O_3 based on variations in weather types in 14 cities. The black lines represent the observed inter-annual MDA8 O_3 trend, whereas the red and blue lines are the trends of reconstructed MDA8 O_3 concentrations according to the frequency-only and both frequency and intensity of weather types changes, respectively. The percentages in each city indicate the O_3 inter-annual variabilities influenced by frequency-only and by both frequency and intensity of weather types changes.

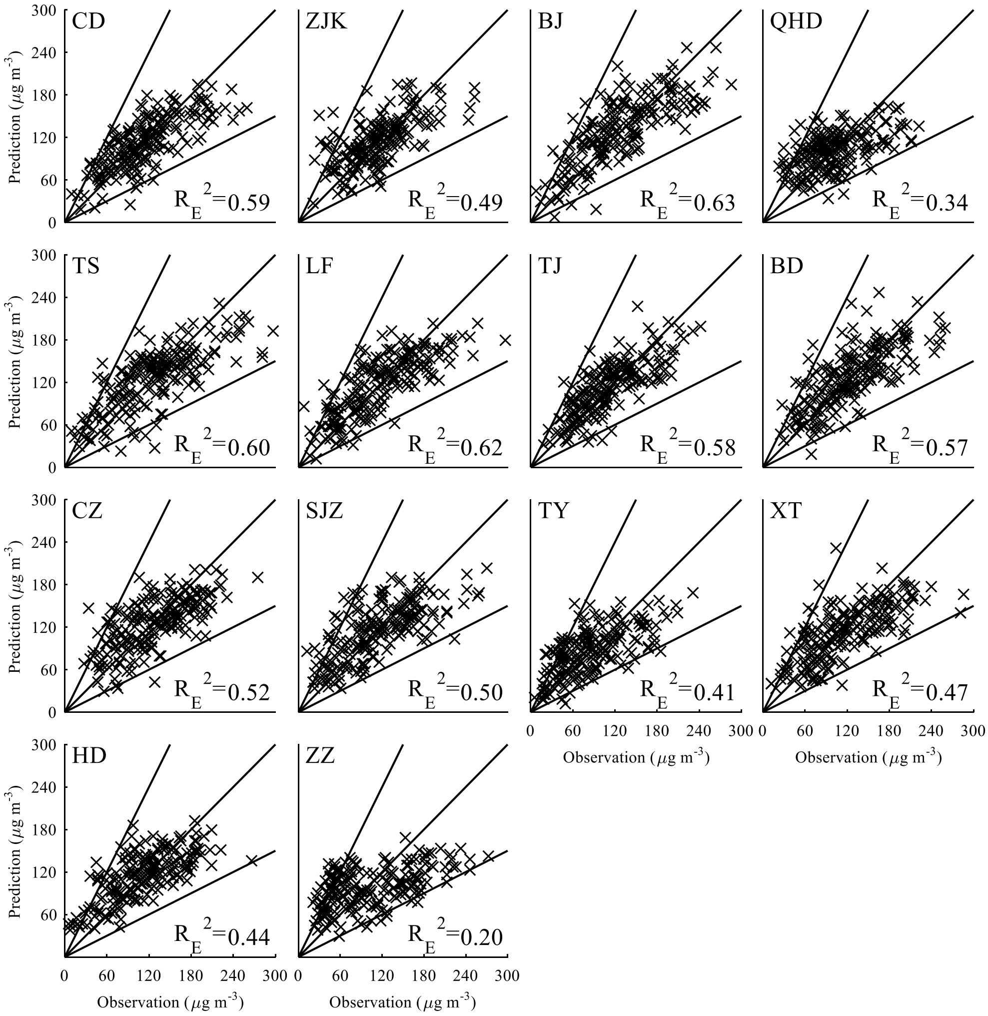

Fig. 9. Scatter plots of predicted versus observed MDA8 O_3 concentrations for each city. The predicted concentrations were obtained by inputting the validation data (20% of the total data) into the corresponding model equations of five weather categories. The R_E^2 values indicate the percentage of explained variance in the composite model that contains the building and validation datasets for each city. The three black lines indicate 2:1, 1:1 and 1:2 ratio lines of predictions and observations.